Chapter 4

A Flexible Virtual Inertia and Damping Control Strategy for Virtual Synchronous Generator for effective utilization of Energy Storage

4.1 Introduction

This chapter presents a flexible inertia and damping control method for VSG for the effective utilization of energy storage. The output power and frequency of the VSG may fluctuate when there is a large variation in the generation from renewable sources. Virtual inertia and damping affect the dynamic response of VSG as well as the cost-effectiveness of energy storage configurations. The virtual inertia of VSG helps to reduce RoCoF of VSG. But even though the optimum values of inertia and damping are used, those parameters are fixed throughout the operation of the VSG. To reduce the oscillatory output of real power and VSG frequency, different adaptive control methods of VSG are proposed in the literature. But the major problem with the existing adaptive control methods is that the extreme values of both VSG parameters have been chosen at different intervals, but there is no explanation for the effect on the other control loops because of the extreme values of

inertia and damping. Furthermore, no analysis that takes into account the energy storage requirement for robust/adaptive control of virtual inertia and damping when designing the parameters of the VSG active power loop has been found in the literature.

The contribution of this chapter is to analyze the simultaneous adjustment of both damping and inertia for better transient characteristics of the power loop of VSG. The effect of parameters on the energy absorbed by the storage unit is analyzed in order to understand its consideration while designing the parameters. Later, A flexible inertia and damping-based control method is depicted to effectively utilize the energy storage system. Further, the proposed control algorithm is compared with the adaptive J control [82], and alternating J and D_P control [87] in terms of energy storage usage.

A brief outline of the chapter is as follows:

- The schematic and operating principle of the considered VSG are depicted in Section 4.2.
- A small signal representation of a virtual synchronous generator is presented in section 4.3.
- Time domain analysis of VSG to find out the effect of parameter variation on active power and frequency is presented in Section 4.4.
- Energy absorbed/supplied by the storage unit with the fluctuation in active power is investigated in detail in section 4.5.
- A flexible control method of virtual inertia and damping of VSG is proposed in Section 4.6.
- This proposed control strategy is simulated in the MATLAB platform, and verified results are discussed in section 4.7.
- Experimental results of the VSG prototype are discussed in Section 4.8.
- The conclusion comes next in section 4.9.

4.2 Block Diagram Representation

The schematic representation of the VSG structure is depicted in Figure 4.1.

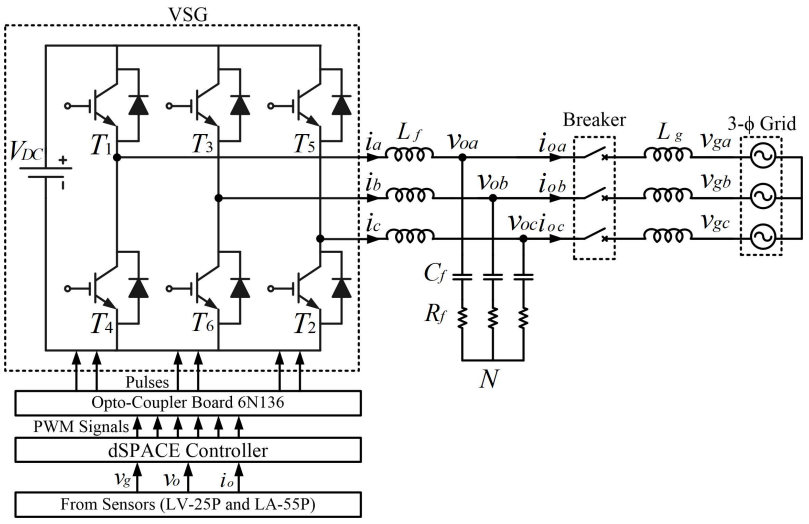

Figure 4.1: Schematic diagram of virtual synchronous generator

The control algorithm for VSG comprises the properties of synchronous generator such as kinetic inertia and damping. Thus, eqns. (4.1)-(4.3) can be used to express the VSG equations. Equations (4.1) and (4.2) reflect the VSG's active power loop, whereas equation (4.3) describes the reactive power loop.

$$T_m - T_e - D_P(\omega - \omega_0) = J\frac{d\omega}{dt} \tag{4.1}$$

$$\frac{P_m}{\omega_0} - \frac{P_e}{\omega} - D_P(\omega - \omega_0) = J\frac{d\omega}{dt} \tag{4.2}$$

$$\sqrt{2}E = k_{iq}\int (Q^* - Q) + \sqrt{2}D_q({V^*}_o - V_o) \tag{4.3}$$

Here, D_P and J denotes the virtual damping and the virtual inertia respectively. Reference or mechanical torque of the VSG is T_m and torque generated by VSG is T_e. VSG rotor angle and angular velocity is denoted by θ and ω respectively. ω_0 is the reference frequency in rad/sec. Reference active power (P_m) and reference frequency (ω_0) are used to calculate reference torque (T_m). VSG output active power (P_e) and frequency (ω) are used to determine the generated electrical torque (T_e). Output voltage reference and actual output voltage are indicated by V_o^* and V_o respectively whereas E stands for the generated voltage reference. Output reactive power and the reference reactive power of VSG are Q and Q^* respectively.

4.3 Small Signal Model Of VSG

The active power control loop's small signal model is produced by equation (4.2) at the static operating points specified in equation (4.4). It is assumed that each state variable, x, has a value of X_n at static condition, with a minor disturbance, $\hat{x}$, i.e.

$$\begin{aligned} \omega_0 = \omega_{0n} + \hat{\omega_0}, \quad P_e = P_{en} + \hat{P}_e, \\ P_m = P_{mn} + \hat{P_m}, \quad \delta = \delta_n + \hat{\delta}, \quad \omega = \omega_n + \hat{\omega} \end{aligned} \tag{4.4}$$

Where, δ is the load angle. Assuming $\hat{\delta}$ is very small, $\sin\hat{\delta} \approx \hat{\delta}$. Since, ω_0 is nearly equal to steady state value, $\widehat{\omega}_0 = 0$.

Applying small signal perturbation in equation (4.2), the small signal model of the active power controller will become as,

$$\frac{\widehat{\delta}(s)}{\hat{P}_m(s) - \hat{P}_e(s)} = \frac{1}{(J\omega_0 s + D_p)\, s} \tag{4.5}$$

Also small signal open loop transfer function of active power can be derived as:

$$\frac{\hat{P}_e(s)}{\widehat{\delta}(s)} = \frac{3V_{on}V_{gn}}{X_s} \tag{4.6}$$

Figure 4.2 illustrates the small signal representation of active power loop of the VSG as shown below,

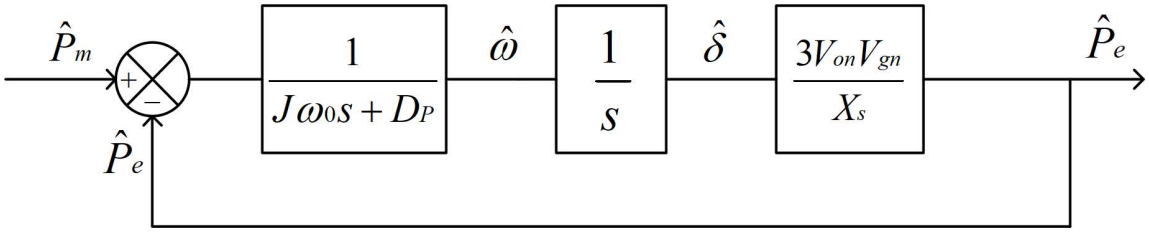

Figure 4.2: Small signal representation of VSG active power loop

4.4 Transient Performance of Active Power Loop of VSG

This section presents the transient response analysis of VSG active power loop. Firstly, mathematical expression of step response of active power is given in Subsection 4.4.1.

Then, transient performance of VSG is analyzed with constant values of inertia and damping in Subsection 4.4.2. Later, transient performance of VSG with respect to variable virtual damping and inertia is analyzed in Subsection 4.4.3 & Subsection 4.4.4 respectively.

4.4.1 Step Response of Active Power and Parameters

Active power to reference power transfer function is derived from Figure 4.2 as,

$$\frac{\hat{P}_e}{\hat{P}_m} = \frac{\frac{K}{J\omega_0}}{s^2 + \frac{D_P}{J}s + \frac{K}{J\omega_0}} \tag{4.7}$$

And VSG frequency to reference power transfer function is derived as,

$$\frac{\hat{\omega}}{\hat{P}_m} = \frac{s}{s^2 + \frac{D_P}{J\omega_0}s + \frac{K}{J\omega_0}} \tag{4.8}$$

where, $K = \frac{3V_{on}V_{gn}}{X_s}$= constant

V_{on} and V_{gn} are nominal output voltage and grid voltage of VSG. X_s denotes the grid impedance. Now natural frequency of oscillation ω_N, damping ratio ζ and damping frequency ω_d of this second order system is given in equation (4.9) as,

$$\begin{aligned} \omega_N &= \sqrt{\frac{K}{J\omega_0}} \text{ and } \zeta = \frac{D_P}{2}\sqrt{\frac{\omega_0}{JK}} \\ \omega_d &= \frac{1}{2J}\sqrt{\frac{4JK - D_P^2\omega_0}{\omega_0}} \\ \phi &= \cos^{-1}\zeta = \cos^{-1}\frac{D_P}{2}\sqrt{\frac{\omega_0}{JK}} \end{aligned} \tag{4.9}$$

Therefore, the step response of active power with change in reference power is given in equation (4.10) as:

$$\hat{P}_e(t) = \hat{P}_m[1 - \frac{e^{-\zeta\omega_N t}}{\sqrt{(1-\zeta^2)}}sin(\omega_d t + \phi)] \tag{4.10}$$

Transient response parameters such as rise time (t_r), peak time (t_p), settling time (t_s) and peak overshoot (M_p) of this system can be given in equation (4.11a)-(4.11c) as follows,

$$t_r = 2J\sqrt{\frac{\omega_0}{4JK - D_P^2\omega_0}}(\pi - \phi) \tag{4.11a}$$

$$t_p = 2\pi J\sqrt{\frac{\omega_0}{4JK - D_P^2\omega_0}} \tag{4.11b}$$

$$t_s = \frac{8J}{D_P}, \quad M_p = e^{-\pi D_P}\sqrt{\frac{\omega_0}{4JK - D_P^2\omega_0}} \tag{4.11c}$$

4.4.2 Virtual damping's impact on the dynamic performance of VSG

Effect of virtual damping coefficient D_P on transient behaviour of active power can be analyzed, by finding the derivative of transient response parameters (t_p, t_s, M_p) with respect to D_P.

From equation (4.11), we can get the derivative of transient response parameter with respect to damping coefficient D_P as,

$$\frac{dt_p}{dD_P} > 0, \quad \frac{dt_s}{dD_P} < 0 \quad \& \quad \frac{dM_p}{dD_P} < 0 \tag{4.12}$$

We can see that peak time is increasing function with respect to D_P, hence the peak time increases with increasing damping coefficient. However, peak overshoot and settling time are decreasing function with respect to D_P. Hence, overshoot and settling time reduces with increasing damping coefficient. Effect of variation of damping on transient response of active power is shown in Figure 4.3.

Similarly, influence of damping coefficient D_P on the VSG frequency can be analyzed using equation (4.8). Peak time, peak overshoot and settling time of frequency, all are decreasing with increasing D_P. Effect of variation of damping on frequency response of VSG is depicted in Figure 4.4.

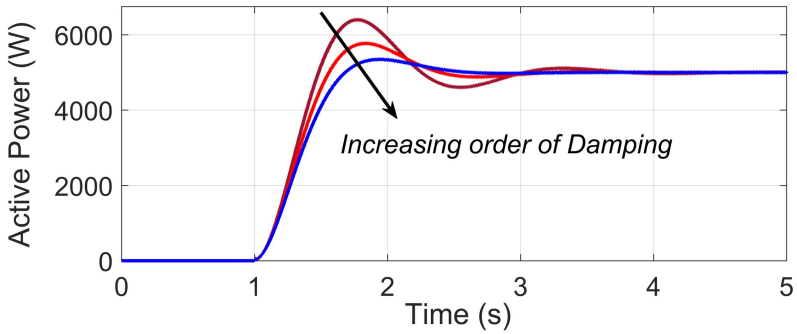

Figure 4.3: Active power response of VSG with variation in damping D_P.

4.4.3 Virtual inertia's impact on the dynamic performance of VSG

Similarly, Effect of virtual inertia (J) on active power can be analyzed by using the derivative of transient performance parameters with respect to J.

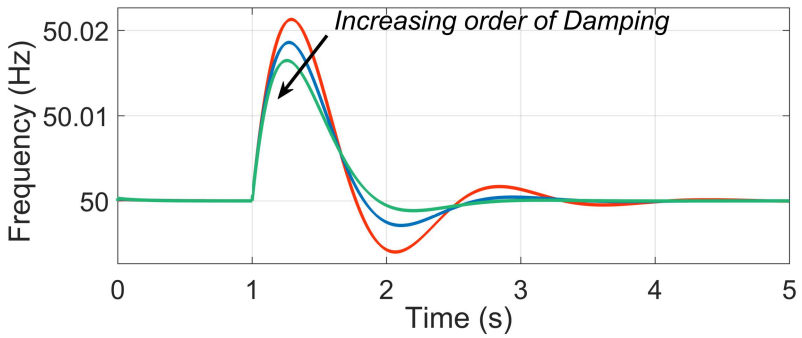

Figure 4.4: Frequency curve of VSG with variation in damping D_P.

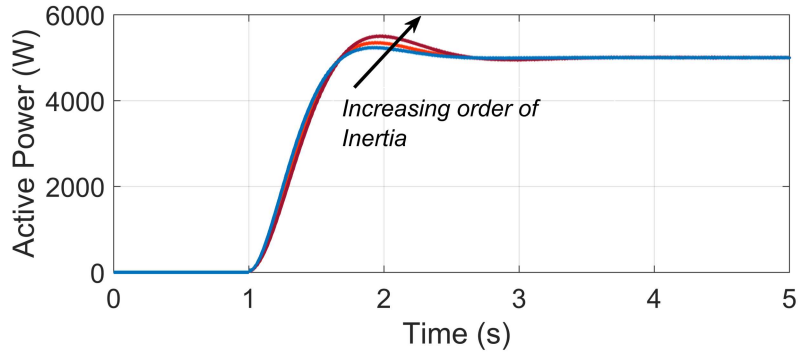

Figure 4.5: Active power response of VSG with variation in virtual inertia J.

From equation (4.11), we can see that,

$$\frac{dt_p}{dJ} > 0, \quad \frac{dt_s}{dJ} > 0 \quad \& \quad \frac{dM_p}{dJ} > 0 \tag{4.13}$$

By the analysis, the peak time of active power, settling time and peak overshoot, are increasing function with respect to J. Hence, peak time, settling time and peak overshoot of active power increases with increasing virtual inertia. The step response of active power with the variation in virtual inertia (J) is shown in Figure 4.5.

Similarly, effect of virtual inertia J on frequency response can be analyzed using equation (4.8). Peak time & settling time of frequency response are increasing with respect to J. However, peak overshoot is decreasing with respect to virtual inertia J. Effect of variation of virtual inertia J on frequency response of VSG is shown in Figure 4.6.

By analyzing the effect of inertia and damping on the dynamic behaviour of VSG, it is observed that both the parameters need to be adjusted for damping out the oscillations properly.

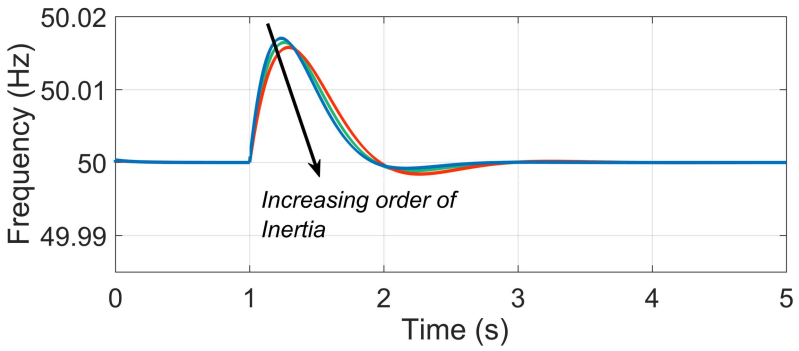

Figure 4.6: Frequency curve of VSG with variation in virtual inertia J.

4.5 Analysis of the Energy Storage

From Eq.(4.10), Step response of active power is given by:

$$\hat{P}_e = \hat{P}_m[1 - \frac{e^{-\zeta\omega_N t}}{\sqrt{(1-\zeta^2)}} sin(\omega_d t + \phi)]$$

The $\hat{P}_m$ represents the step change in the reference value of active power, and the area confined between $\hat{P}_m$ and $\hat{P}_e$ denotes the energy consumed/supplied by the DC storage unit. Hence, the energy consumed/supplied by the storage segment is calculated as,

$$\begin{aligned} E(t) &= \int_0^t [\hat{P}_m - \hat{P}_e(t)]dt \\ &= \hat{P}_m \frac{e^{-\zeta\omega_N t}}{\omega_N}[\cos(\omega_d t + \phi) + \frac{\zeta}{\sqrt{1-\zeta^2}} \sin(\omega_d t + \phi)] \end{aligned} \tag{4.14}$$

The following section discusses, the energy absorbed by the storage segment for both critically damped and under-damped system.

Case I: For critically damped system ($\zeta = 1$)

Energy absorbed for critically damped system can be expressed as equation (4.15) by substituting $\zeta = 1$ in equation (4.14):

$$E(t) = \frac{\hat{P}_m}{\omega_N}[2 - 2e^{-\omega_N t} - \omega_N t e^{-\omega_N t}] \tag{4.15}$$

For critically damped system, total amount of energy that the storage segment needs to absorb during the disturbance in real power is computed by keeping t$\rightarrow\infty$.

$$E(\infty) = \frac{2\hat{P}_m}{\omega_N} \tag{4.16}$$

Figure 4.7 shows the energy absorbed/supplied by the storage device in case of critically damped system for the step response of active power.

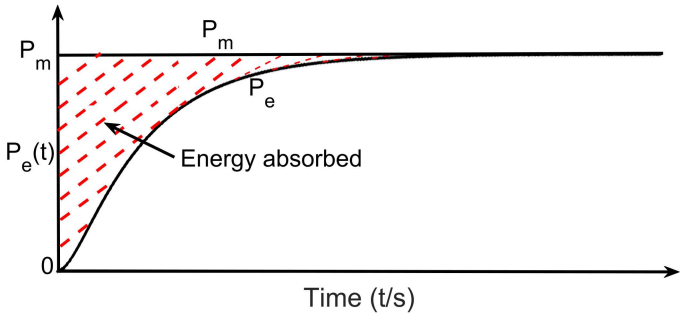

Figure 4.7: Active power of VSG for critically damped system

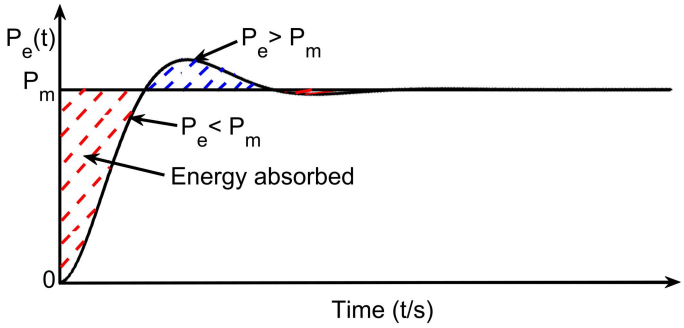

Figure 4.8: Active power of VSG for under-damped system

Case II: For under-damped system ($0 < \zeta < 1$)

Hence, total energy absorbed by the storage device until the active power reaches to equilibrium state for the very first time i.e. rise time, is derived by substituting $t = t_r$ in the above expression.

$$E(t_r) = \hat{P}_m \frac{e^{-\zeta\omega_N t_r}}{\omega_N}[\cos(\omega_d t_r + \phi) + \frac{\zeta}{\sqrt{1-\zeta^2}}\sin(\omega_d t_r + \phi)] \tag{4.17}$$

Total Energy absorbed in case of under-damped system is calculated by substituting $t_r = (\pi - \phi)/\omega_d$ as,

$$E = \frac{\hat{P}_m}{\omega_N} e^{\frac{-\zeta(\pi-\phi)}{\sqrt{1-\zeta^2}}} \tag{4.18}$$

Equation (4.18) provides the energy required for sizing of the storage device for the under-damped scenario when the real power disturbances occur. Energy absorbed by the storage unit in case of under-damped system is shown by step response of active power in the Figure 4.8.

According to the above analysis, there is no overshoot in the active power output when the system is critically damped, but the system responds slowly and requires more energy storage than an under-damped system does. So, there is a trade-off between under-

damping and critically damping system while designing the energy storage. Therefore, to reduce the energy storage requirement, the design of the system needs to be slightly under-damped ($\zeta = 0.707$) with power oscillations kept within acceptable limits.

4.6 Proposed Flexible Virtual Inertia and Damping Control

In this section, the proposed control algorithm is designed by using energy storage requirement and adaptive virtual inertia and damping. By using Eq. (4.14), energy of the storage unit is,

$$E(t) = \int_0^t [\hat{P}_m - \hat{P}_e(t)]dt$$

Using small signal perturbation,

$$\omega = \omega_n + \hat{\omega}, \quad \omega_0 = \omega_{0n} + \hat{\omega_0}, \quad E = E_0 + \hat{E} \tag{4.19a}$$

$$J = J_0 + \hat{J}, \quad D_P = D_{P0} + \hat{D_P} \tag{4.19b}$$

Using equation (4.19a)-(4.19b), derivative of E from equation (4.14) can be written as below:

$$\frac{d(\hat{E})}{dt} = \hat{P_m} - \hat{P_e}(t) \tag{4.20}$$

Energy stored by virtual rotor can be expressed as,

$$E = \frac{1}{2}J\omega^2 \tag{4.21}$$

$$\frac{dE}{dt} = \frac{d}{dt}(\frac{1}{2}J\omega^2) \tag{4.22}$$

From equation (4.20), the equation (4.22) can be rewritten as,

$$\frac{d\hat{E}}{dt} = J_0\omega_n\frac{d}{dt}\hat{\omega} + \frac{1}{2}\omega_n^2\frac{d\hat{J}}{dt} \tag{4.23}$$

Substituting the value of $\frac{d(\hat{E})}{dt}$ from equation (4.20) into equation (4.23) gives the expression as given in equation (4.24),

$$\hat{P_m} - \hat{P_e} = J_0\omega_n\frac{d}{dt}\hat{\omega} + \frac{1}{2}\omega_n^2\frac{d\hat{J}}{dt} \tag{4.24}$$

Applying perturbation in equation (4.2) we get,

$$(\hat{P_m} - \hat{P_e}) - D_P(\omega_0\hat{\omega}) = J\omega_0\frac{d\omega}{dt} \tag{4.25}$$

Substituting the value of $\hat{P_m} - \hat{P_e}$ from (4.24) into the equation (4.25), we get the relation as given in equation (4.26),

$$\begin{aligned} J_0\omega_n\frac{d\hat{\omega}}{dt} + \frac{1}{2}\omega_n^2\frac{d\hat{J}}{dt} - (D_{P0} + \hat{D_P})(\omega_{0n} + \hat{\omega_0})\hat{\omega} \\ = (J_0 + \hat{J})(\omega_{0n} + \hat{\omega_0})\frac{d(\omega_n + \hat{\omega})}{dt} \end{aligned} \tag{4.26}$$

Then by simplifying the equation (4.26) by neglecting the dc terms and product of the small variations, we get equation (4.27) as,

$$\frac{1}{2}\omega_{0n}^2\frac{d\hat{J}}{dt} = D_{P0}\omega_{0n}\hat{\omega} \tag{4.27}$$

Solving the equation (4.27), variable inertia is derived as given in the equation (4.28),

$$\hat{J} = \frac{2D_{P0}}{\omega_{0n}}\hat{\delta} \tag{4.28}$$

Since, damping ratio of the second order active power transfer function of equation (4.7) is $\zeta = \frac{D_P}{2J\omega_n}$. Hence, D_P can be rewritten as given in equation (4.29),

$$D_P = 2J\zeta\omega_N \tag{4.29}$$

Substituting the values of D_P and J from equation (4.19b) into (4.29) and ignoring the dc terms, expression for variable damping is derived as given in equation (4.30),

$$\hat{D_P} = 2\zeta(\hat{J}\omega_{N0} + J_0\hat{\omega_N}) \tag{4.30}$$

$$\text{where,} \quad \omega_{N0} = \sqrt{\frac{K}{J_0\omega_{0n}}} \tag{4.31}$$

From equation (4.28) and (4.30), the desired value of flexible virtual inertia and damping are calculated as,

$$J = J_0 + \hat{J}, \qquad D_P = D_{P0} + \hat{D_P} \tag{4.32}$$

Where, J_0 and D_{P0} are steady state values of virtual inertia and virtual damping respectively. D_{P0} is determined based on the grid code. According to [42], 2% change in grid frequency causes 100% change in real power. J_0 is determined by putting D_{P0}

into equation (4.9). Proposed control method for VSG is shown in Fig. 4.9. Flexible J and D_P values are updated according to Eqn.(4.32) as shown in Figure 4.9 (a). Complete control algorithm of VSG is shown in Figure 4.9 (b).

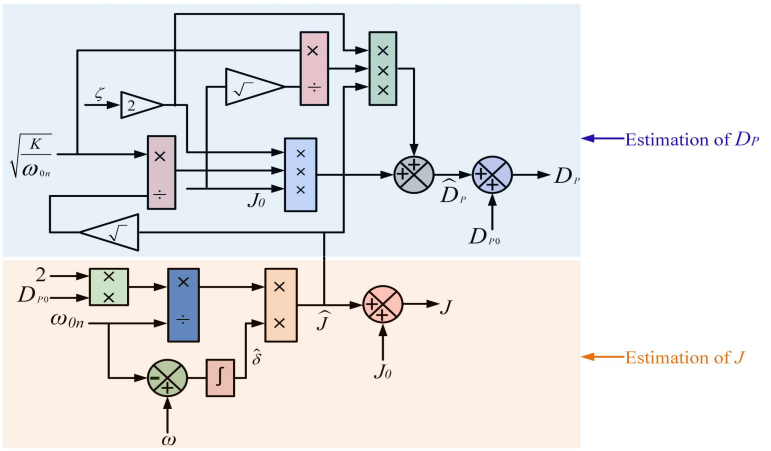

(a)

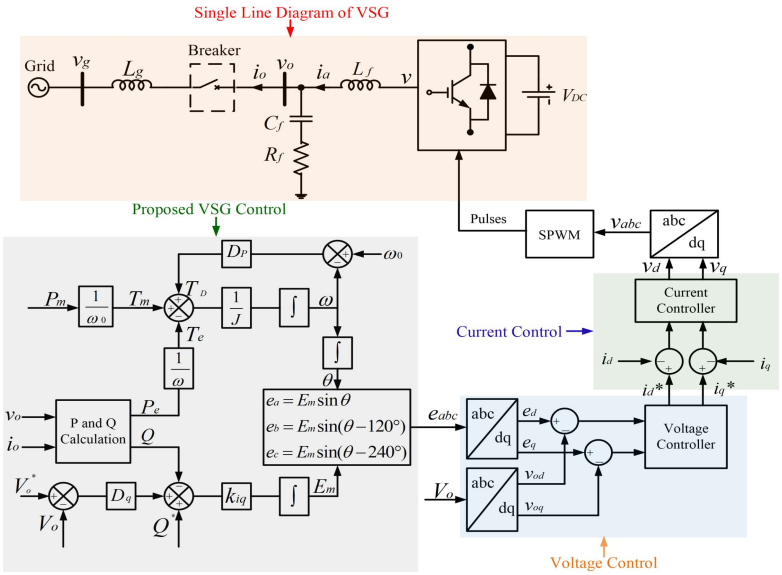

(b)

Figure 4.9: Proposed Control method of VSG (a) Estimation of adaptive J and D_P (b) Complete VSG control algorithm

4.7 Simulation Results

The proposed control algorithm is simulated using MATLAB/simulink environment. Simulation parameters are shown in Table 4.1. At first, the proposed control algorithm is verified with the simulation results. Later, the proposed control strategy is compared with the adaptive J control [82] and Alternating J and D_P control [87] of VSG.

Table 4.1: Simulation Parameters

S.No.	Parameter	Values
1	DC Voltage	220 V
2	3-ϕ ac Voltage	110 $V/50$ Hz
3	Interfacing Inductance (L_f)	3.5 mH
4	Steady State Virtual Inertia (J_0)	0.1 $kg-m^2$
5	Steady State Virtual damping (D_{P0})	5

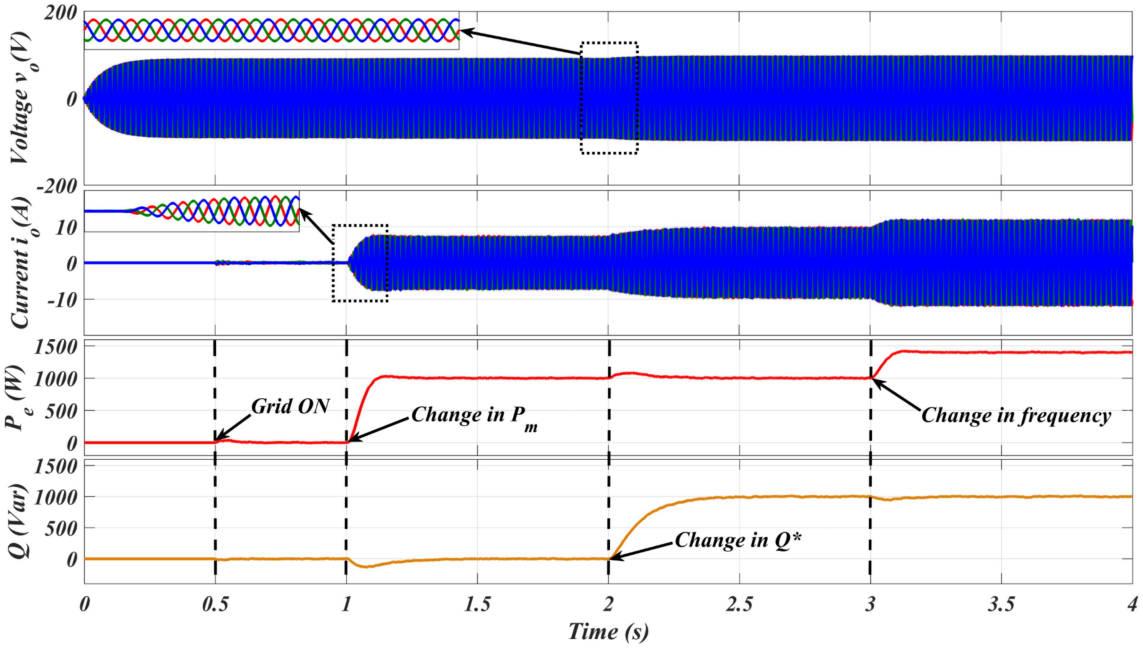

Figure 4.10: VSG response with the proposed control method

4.7.1 Simulation results of the proposed control algorithm

The developed VSG control algorithm is tested for the synchronization, variation in reference active power, reference reactive power and grid frequency. Response of the VSG voltage v_o, current i_o, real power P_e and reactive power Q with proposed control method is shown in Figure 4.10. Simulation results are explained in the following subsections.

4.7.1.1 Synchronization

From $t = 0$ seconds, as shown in Figure 4.11, VSG is working in islanded mode and maintains constant output voltage and frequency. At $t = 0.5$ seconds, circuit breaker is turned on and VSG is connected to the grid smoothly. So, there is no change in VSG output voltage and current before and after grid connection as shown in Figure 4.11. At 1 s, the active power is changed from 0 to 1 kW. So, the current starts increasing at 1 s. as shown in Figure 4.12.

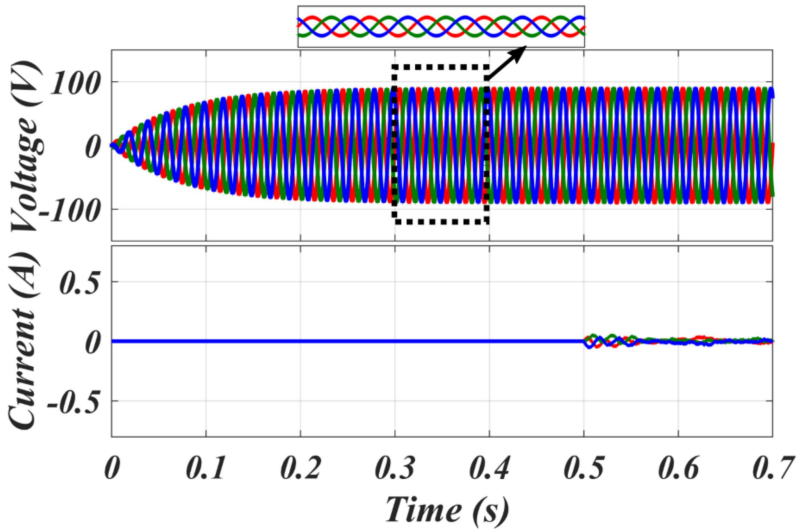

Figure 4.11: VSG voltage and current while grid connection

The steady state current, voltage at power reference of 1 kW are shown in Figure 4.13.

4.7.1.2 Change in reference active power, reactive power and grid frequency

Initially, active and reactive power reference was set to zero i.e. $P_m = 0$ & $Q^* = 0$. At $t = 1$ seconds, active power reference P_m to the grid is changed from 0 to 1 kW. Active

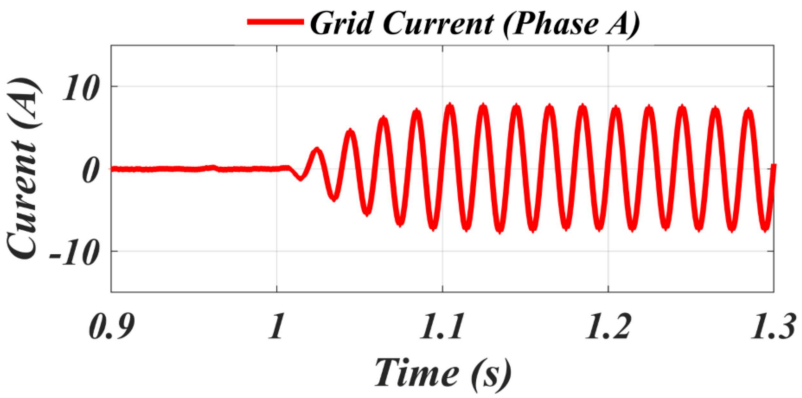

Figure 4.12: Grid current i_{oa} of proposed control

power P_e of VSG follows the reference power P_m with some oscillations and delay due to virtual damping and inertia as shown in Figure 4.14. Hence, VSG fulfils the active power demand of the grid without affecting reactive power flow.

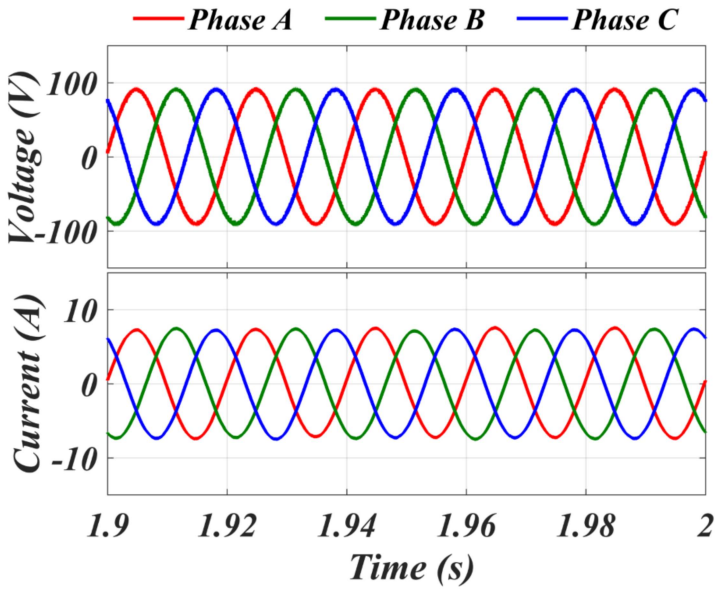

Figure 4.13: Output voltage and current of VSG with proposed method

At $t = 2$ seconds, the reference reactive power Q^* is set to 1 kVar. So, VSG supplies 1 kVar reactive power to the grid as shown in Figure 4.14. While, active power of VSG is observed to be almost no change.

At $t = 3$ seconds, grid frequency was decreased from its nominal value i.e. 50 Hz to 49.8 Hz. During this time, VSG supplies active power to the grid even the active power reference was not changed. Hence, VSG participates in frequency regulation process by

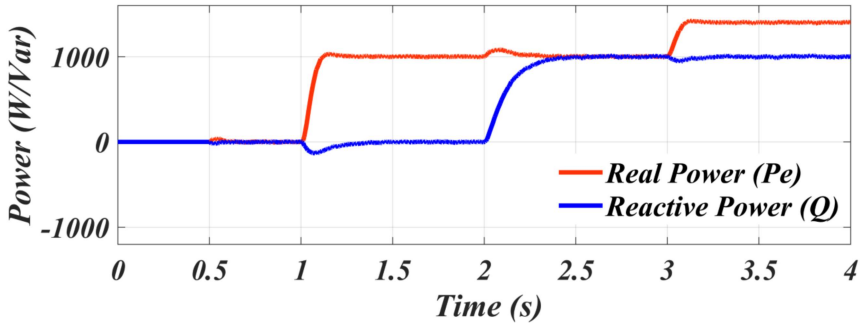

Figure 4.14: Variation in active power (P_e) and Reactive power (Q) with change in reference active power (P_m), reference reactive power (Q^*) and grid frequency ω_g

supplying active power to the grid. Reactive power supplied by VSG does not change because, it is not dependent on frequency. Simulation was stopped at $t = 4$ seconds.

4.7.2 Comparison with the adaptive J control and Alternating J and D_P control

The results of the proposed control method are compared with the already existing adaptive J control [82] and alternating J and D_P control [87] and are presented in Figure (4.15)-(4.16). Figure 4.15 presents the variation in active power for all three cases with the step change of 1 kW in reference active power. From Figure 4.15, one can observe that, the proposed control method has shown less peak overshoot and less settling time. Figure 4.16 presents the variation in frequency of the VSG for all three cases when there is a step change in reference active power. It is observed that proposed control method shows minimum frequency deviation from the steady state and shows the shortest settling time than other two adaptive control methods.

Figure 4.15 demonstrates that adaptive J control has the maximum overshoot of 440 W and the longest settling time of 0.9 s. Comparing with the existing adaptive J control of VSG, alternating J and D_P control shows significant reduction in the overshoot and settling time with only 180 W overshoot and 0.6 s settling time. So, alternating J and D_P control method is effective in reducing the power fluctuations. However, the proposed adaptive control method shows the least overshoot of 40 W and settling time of 0.3 s as compared to other two methods. Hence, proposed control method gives the best active power response of VSG.

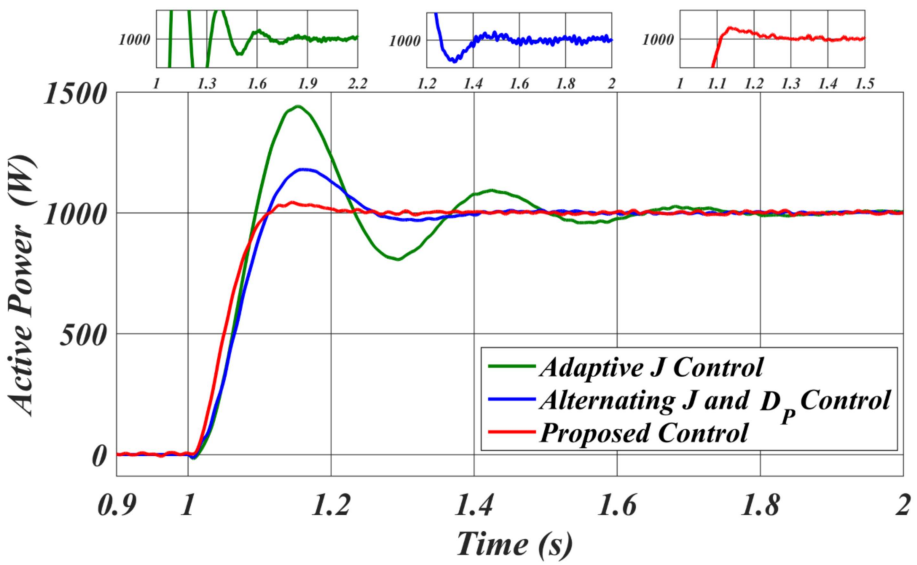

Figure 4.15: Output power of VSG

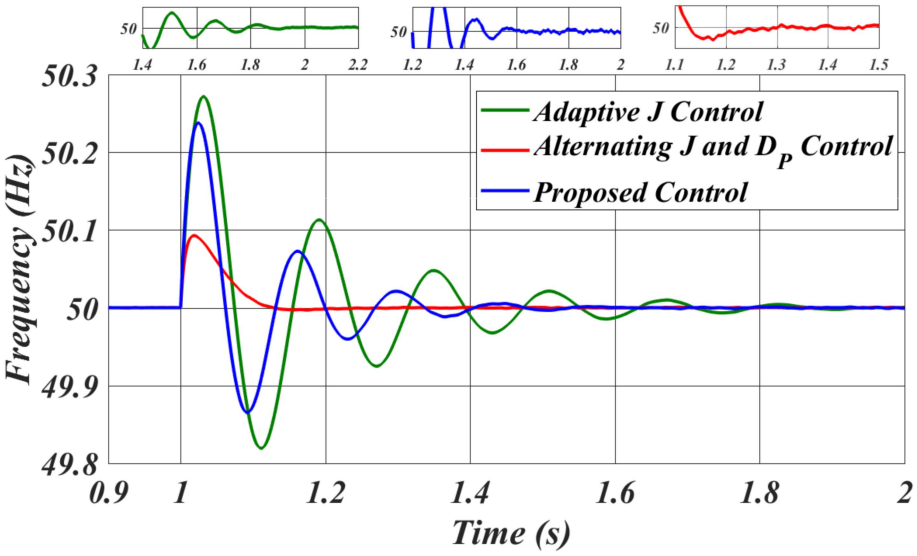

Figure 4.16: Output frequency of VSG

Also, the adaptive J control has larger frequency variation of 0.275 Hz and longer settling time of 0.9 s, while the proposed method is most effective in suppressing the frequency transients. Alternating J and D_P control reduces the frequency deviation to 0.24 Hz in comparison to adaptive J control of VSG. Settling time of frequency is also reduced to 0.6 s. Hence, frequency oscillations are reduced and frequency is restored quickly as compared to adaptive J control of VSG. In addition, with the proposed adaptive control method, frequency deviation is further reduced to 0.09 Hz as compared to the

alternating J and D_P control of VSG. Settling time of frequency is further reduced to 0.3 s which, shows the effectiveness of proposed control method.

Comparison of the proposed control method with the existing adaptive control methods with respect to different parameters i.e. peak overshoot, settling time and energy supplied by the storage element is shown in Table 4.3. Comparison of the proposed method with the other two control methods considering the qualitative issues such as implementation complexity, size of the storage element etc. is presented in Table 4.4.

Since, the oscillations in the active power and frequency of VSG is minimum in the proposed flexible method as compared to the other two adaptive control methods, the energy absorbed/supplied by the storage element is minimum in the proposed method as shown in Table 4.3. As a result, the size of the storage element is reduced.

4.8 Experimental Results

4.8.1 Experimental results with proposed Algorithm

The transient behaviour of the VSG is recorded using digital oscilloscope (KEYSIGHT infiniiVision DSOX2004A). Experimental parameters are shown in Table 4.2. The experimental results of the proposed VSG are presented in this section to show its superiority for both steady state and dynamic conditions.

Table 4.2: Experimental Parameters

S.No.	Parameter	Values
1	DC Voltage	220 V
2	3-ϕ ac Voltage	110 $V/50$ Hz
3	Interfacing Inductance (L_f)	3.5 mH
4	Steady State Virtual Inertia (J_0)	0.1 $kg-m^2$
5	Steady State Virtual damping (D_{P0})	5

4.8.1.1 Synchronization

Initially, VSG is working in islanded mode. For grid connection of VSG, synchronization control is activated to synchronize the output voltage of VSG with the grid voltage.

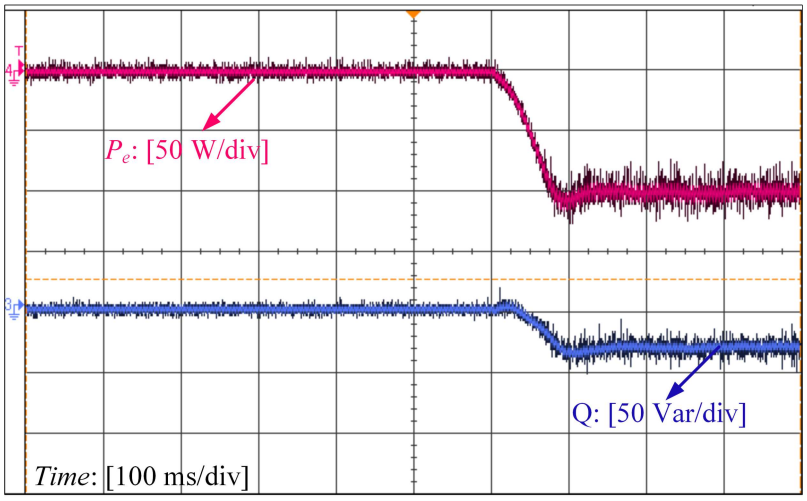

Figure 4.17: Active power P_e and reactive power Q of VSG after grid connection

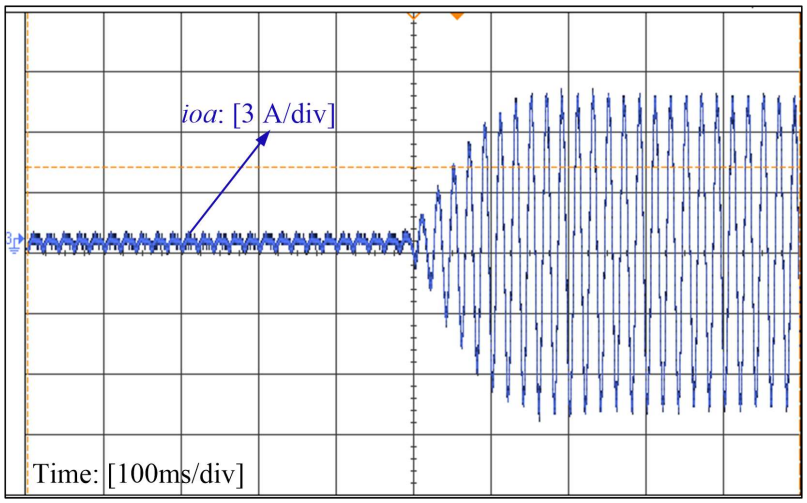

Figure 4.18: Grid current waveform with proposed method

After synchronization, VSG is connected to the grid and because of variation in grid frequency and voltage amplitude, VSG exchanges some amount of active and reactive power with the grid as shown in Figure 4.17. At this instant, the grid frequency is more than 50 Hz. Hence, VSG absorbs the active power from the grid, as shown in Figure 4.17.

The VSG output current/grid current i_{oa} with proposed method when output power P_e changes from 0 to 1 kW is shown in Figure 4.18. Three phase line voltages and current waveforms of VSG after it reaches to steady state are shown in Figure 4.19.

Then, VSG is tested for its dynamic performance by changing its reference active

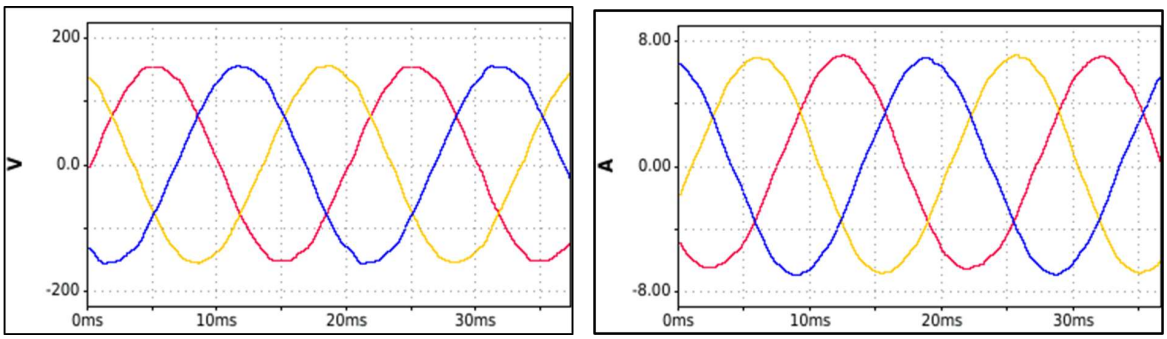

(a) (b)

Figure 4.19: Output voltage and current waveforms of VSG (a) v_{oab}, v_{obc} and v_{oca} (b) i_{oa}, i_{ob} and i_{oc}

Table 4.3: Comparison of proposed control with existing literature

	Active Power		Frequency		Energy supplied
	Overshoot	Settling Time	Overshoot	Settling Time	
Adaptive J Control [82]	440 W	0.9 s	0.275 Hz	0.9 s	60 $Joule$
Alternating J and D_p Control [87]	180 W	0.6 s	0.24 Hz	0.6 s	56 $Joule$
Proposed Control	40 W	0.3 s	0.09 Hz	0.3 s	47 $Joule$

Table 4.4: Qualitative comparison of proposed control with existing literature

	Implementation	Storage Size
Adaptive J Control [82]	Complex	Big
Alternating J and D_p Control [87]	More complex	Medium
Proposed Control	Less complex	Small

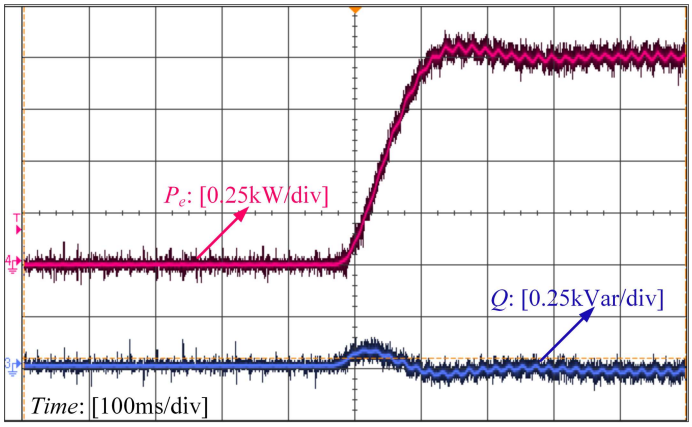

Figure 4.20: Change in active power P_e with the reference active power P_m

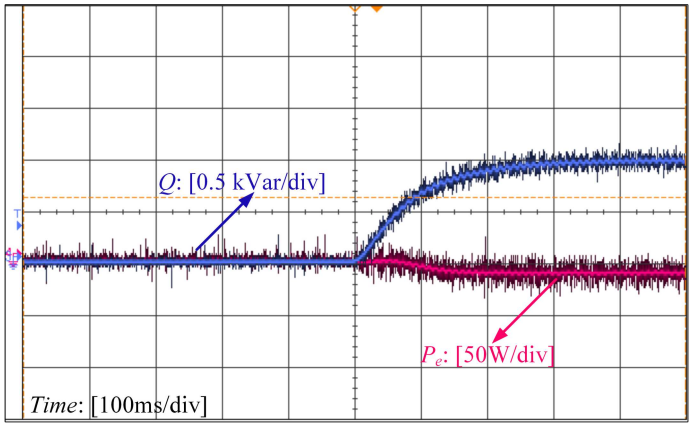

Figure 4.21: Change in reactive power Q with the reference reactive power Q^*

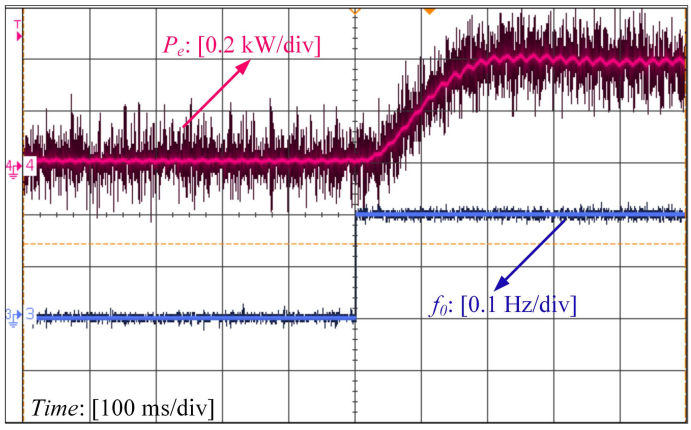

Figure 4.22: Change in active power P_e with VSG reference frequency

and reactive powers and changing the VSG reference frequency, as discussed in the next subsection.

4.8.1.2 Change in reference active Power (P_m), reference reactive power (Q^*) and reference frequency (ω_0)

Initially, active power reference P_m to the grid is increased from 0 to 1 kW as depicted in Figure 4.20, the active power exchange between VSG and grid starts occurring and there is no change in reactive power.

Now, reactive power reference Q^* to the grid is changed from 0 to 1 kVar assuming that there is no variation in active power reference, and frequency. VSG quickly supplies the reactive power Q according to the reference reactive power command as shown in Figure 4.21.

The VSG is verified for the frequency regulation by changing the VSG reference frequency ω_0 (f_0 in Hz). VSG performs the frequency regulation by supplying or absorbing the real power to/from the grid. As the grid frequency can't be changed, the change in frequency is emulated by changing the VSG reference frequency. Variation of real power generated from VSG, when reference frequency f_0 is increased by 0.2 Hz, is shown in Figure 4.22.

4.8.2 Comparison of the proposed adaptive control with adaptive J control and Alternating J and D_P control

VSG is tested with all three control methods i.e. adaptive J control [82], alternating J and D_P control [87] and proposed adaptive control and results are compared as shown in Figure 4.23.

The dynamic response of the VSG active power P_e and VSG frequency ω (f in Hz) are recorded for step change of a 1 kW in reference active power. Figure 4.23 (a), 4.23 (b) and 4.23 (c) shows the step response of power and frequency with adaptive J control, alternating J and D_P control and the proposed flexible inertia and damping control.

From Figure 4.23, it is observed that experimental results validate the superiority of the proposed control method in terms of the reduced size of the storage device and less peak overshoot, less settling time in active power and frequency response as compared to the adaptive J control and alternating J and D_P control of VSG.

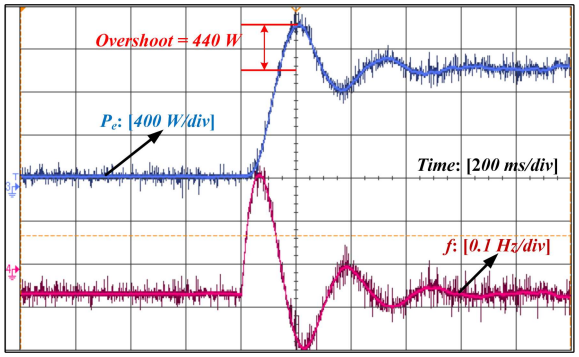

(a)

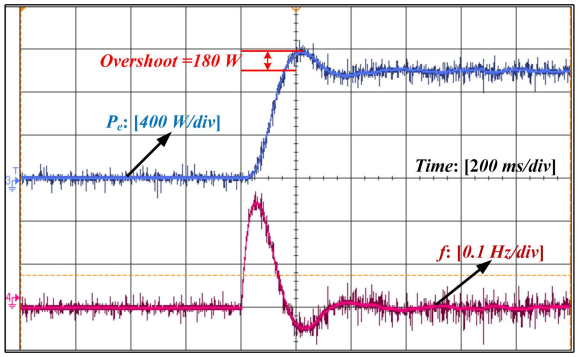

(b)

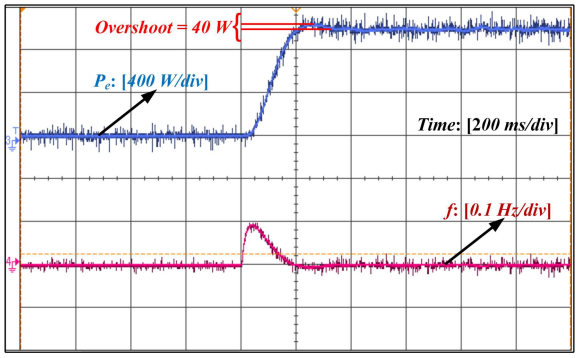

(c)

Figure 4.23: VSG output power and frequency response for a sudden change in the active power reference for (a) adaptive J control [82] (b) alternating J and D_P control [87] (c) proposed adaptive control

4.9 Conclusion

Initially, the effect of variation of inertia and damping on VSG active power and frequency has been analyzed and it was established that frequency and active power oscillations can be vanquished by a bigger damping coefficient and a bigger inertia can take care of the

rate of change of frequency as well as the oscillations in the active power. Further, it is concluded that there is a need to adjust both virtual inertia and damping together to improve the transient response of VSG active power loop. Energy absorbed/supplied by the storage unit was analyzed for both critically damped and under-damped system and observed that for an under-damped system, the energy storage requirement is lesser as compared to critically damped system. So, damping ratio and parameters of the VSG active power loop should be chosen to achieve under-damped response to reduce the energy storage requirements.

A flexible virtual inertia and damping control strategy for VSG for optimizing the energy storage was proposed in this chapter. Proposed scheme was simulated in MATLAB/Simulink platform and also verified on a developed VSG experimental setup. Experimental results of the proposed control method was compared with the adaptive J control and alternating J and D_P control of VSG for a sudden change in the active power reference. Active power of VSG with the proposed control method have the best performance with 40 Watts overshoot and settling time of 0.3 seconds. In addition, VSG frequency shows best response with the proposed control method having least settling time of 0.3 seconds and overshoot of 0.09 Hz. Energy supplied by the storage unit with the proposed control method is also minimum and around 47 $Joule$. Hence, the proposed control method utilizes minimum energy storage and significantly reduces the output frequency deviation and settling time as compared to the other two methods. Further, active power oscillations were also reduced compared to other two control methods while reducing the settling time as well. Future research can be done for the multi-VSG system with the proposed adaptive control. Moreover, adaptive control of VSG under distorted grid condition can also be explored.